



# Generalized pupil function of a compound X-ray refractive lens

SERGEY GASILOV,<sup>1,\*</sup> TOMY DOS SANTOS ROLO,<sup>2</sup> ALBERTO MITTONE,<sup>3</sup>  
SERGEY POLYAKOV,<sup>4</sup> SERGEY TERENTYEV,<sup>4</sup> TOMAS FARAGO,<sup>2</sup> VLADIMIR  
BLANK,<sup>4</sup> ALBERTO BRAVIN,<sup>3</sup> AND TILO BAUMBACH<sup>2</sup>

<sup>1</sup>Canadian Light Source, 44 Innovation Blvd, Saskatoon S7N 2V3, Canada

<sup>2</sup>Karlsruhe Institute of Technology, 1 Hermann von Helmholtz Platz, Eggenstein 76344, Germany

<sup>3</sup>European Synchrotron Radiation Facility, 71 Avenue des Martyrs, Grenoble 38000, France

<sup>4</sup>Technological Institute for Superhard and Novel Carbon Materials, 7a Tsentralnaya, Troitsk 142190, Russian Federation

\*[sergey.gasilov@lightsources.ca](mailto:sergey.gasilov@lightsources.ca)

**Abstract:** Quality of a refractive compound X-ray lens can be limited by imperfections in surfaces of unit lenses and stacking precision. In general case both the lens transmission and optical aberrations define properties of a beam in the lens exit plane; together they can be expressed in terms of the generalized pupil function. In this work we measure this function for a diamond single crystal compound refractive lens. Consequently, we apply the pupil function to evaluate the performance of the examined compound refractive X-ray lens. A number of practically important conclusions can be drawn from such analysis.

© 2017 Optical Society of America

**OCIS codes:** (340.0340) X-ray optics; (220.3630) Lenses; (120.5050) Phase measurement; (220.1010) Aberrations (global).

## References and links

1. A. Snigirev, V. Kohn, I. Snigireva, A. Souvorov, and B. Lengeler, "Focusing high-energy x rays by compound refractive lenses," *Appl. Opt.* **37**(4), 653–662 (1998).
2. B. Lengeler, J. Tümmler, A. Snigirev, I. Snigireva, and C. Raven, "Transmission and gain of singly and doubly focusing refractive x-ray lenses," *J. Appl. Phys.* **84**(11), 5855–5861 (1998).
3. A. Snigirev, Y. Yunkin, I. Snigireva, M. Di Michiel, M. Drakopoulos, S. Kouznetsov, L. Shabel'nikov, M. Grigoriev, V. Ralchenko, I. Sychoy, M. Hoffmann, and E. I. Voges, "Design and microfabrication of novel X-ray optics," *Proc. SPIE* **4783**, 1–9 (2002).
4. S. Terentyev, V. Blank, S. Polyakov, S. Zholudev, A. Snigirev, M. Polikarpov, T. Kolodziej, J. Qian, H. Zhou, and Y. Shvyd'ko, "Parabolic single-crystal diamond lenses for coherent x-ray imaging," *Appl. Phys. Lett.* **107**(11), 111108 (2015).
5. P. Heimann, M. MacDonald, B. Nagler, H. J. Lee, E. Galtier, B. Arnold, and Z. Xing, "Compound refractive lenses as pre-focusing optics for X-ray FEL radiation," *J. Synchrotron Radiat.* **23**(2), 425–429 (2016).
6. J. W. Goodman, *Introduction to Fourier Optics*, 3rd ed. (Roberts and Company Publishers, 2005).
7. S. Rutishauser, I. Zanette, T. Weitkamp, T. Donath, and C. David, "At-wavelength characterization of refractive x-ray lenses using a two-dimensional grating interferometer," *Appl. Phys. Lett.* **99**(22), 221104 (2011).
8. A. Momose, W. Yashiro, and Y. Takeda, "X-Ray Phase Imaging with Talbot Interferometry," in *Imaging, Therapy Planning, and Inverse Problems in Biomedical Mathematics: Promising Directions* (Medical Physics Publishing, 2009), p. 292.
9. T. Weitkamp, B. Nöhammer, A. Diaz, C. David, and E. Ziegler, "X-ray wavefront analysis and optics characterization with a grating interferometer," *Appl. Phys. Lett.* **86**(5), 054101 (2005).
10. F. J. Koch, C. Detlefs, T. J. Schröter, D. Kunka, A. Last, and J. Mohr, "Quantitative characterization of X-ray lenses from two fabrication techniques with grating Interferometry," *Opt. Express* **24**(9), 9168–9177 (2016).
11. C. M. Slack, "The refraction of X-rays in prisms of various materials," *Phys. Rev.* **27**(6), 691–695 (1926).
12. M. N. Wernick, O. Wirjadi, D. Chapman, Z. Zhong, N. P. Galatsanos, Y. Yang, J. G. Brankov, O. Oltulu, M. A. Anastasio, and C. Muehleman, "Multiple-image radiography," *Phys. Med. Biol.* **48**(23), 3875–3895 (2003).
13. S. Gasilov, A. Mittone, E. Brun, A. Bravin, S. Grandl, A. Mirone, and P. Coan, "Tomographic reconstruction of the refractive index with hard X-rays: an efficient method based on the gradient vector-field approach," *Opt. Express* **22**(5), 5216–5227 (2014).
14. J. C. Wyant and K. Creath, "Basic wavefront Aberration theory for Optical Metrology," *Appl. Opt. Opt. Eng.* **11**, 2–53 (1992).

15. F. Seiboth, A. Schropp, M. Scholz, F. Wittwer, C. Rödel, M. Wünsche, T. Ullsperger, S. Nolte, J. Rahomäki, K. Parfeniukas, S. Giakoumidis, U. Vogt, U. Wagner, C. Rau, U. Boesenberg, J. Garrevoet, G. Falkenberg, E. C. Galtier, H. Ja Lee, B. Nagler, and C. G. Schroer, "Perfect X-ray focusing via fitting corrective glasses to aberrated optics," *Nat. Commun.* **8**, 14623 (2017).</jrm>

## 1. Introduction

An X-ray refractive lens is composed of tens of unit lenses aligned along the optical axis. One of the most frequent applications of such compound X-ray refractive lenses (CRL) is in focusing of the X-ray beams [1]. The focal spot size and the intensity gain are two important parameters that depend on the CRL quality. Normally, they are expressed in terms of the CRL transmission and its effective aperture, which are related to the attenuation of X-rays in the CRL [2]. The effective aperture provides an assessment of CRL properties under the assumption that it is an aberration-free optical system. In general, however, the CRL geometry is not perfect due to the relative misalignment of unit lenses or systematic errors in the unit lens surface shape. An example is a CRL made of diamond. Owing to its outstanding thermal conductivity, it is a particularly suitable material for the implementation of CRLs for the collimation and focusing of high-power X-ray beams produced by conventional and XFEL undulators [3–5]. However, due to the complexity of the micromachining procedure of the diamond (ablation by ultrafast laser pulses) the geometry of unit lenses is not perfect. The performance of the very first diamond-based CRLs has not fully met the design expectations. It was reported that a demagnified image of an X-ray source appeared to be at least twice broader than the one expected from the estimates and measurements of the CRL transmission [4]. One can assume that optical aberrations limit the performance of diamond-based CRLs. In this work we suggest a way to measure optical aberrations of an X-ray CRL and to construct its generalized pupil function. This approach can be used to get information about the manufacturing imperfections and to assess the focusing and imaging properties of a refractive X-ray lens, such as its point spread function.

The generalized pupil function  $P(x, y) = \sqrt{T} e^{i\phi}$  is a complex transmission function of coordinates  $(x, y)$  in the lens exit plane; in the hard X-ray spectral range it is also a function of the X-ray energy  $E$ . The square of its absolute value provides information about the transmitted intensity of light  $T$ , while its phase  $\phi$  shows to which extent the real aberrated wavefront differs from ideal parabolic shape [6]. The latter is an essential quantity that alters the position of the circle of least confusion, the gain, and other properties of a photon beam focused by a real, imperfect lens. Several methods commonly known as X-ray phase contrast techniques can be used to measure wavefront curvatures in the hard X-ray spectral range. In particular, grating interferometry is a phase-sensitive technique that has been previously applied to the characterization of X-ray beam wavefront downstream of an X-ray lens [7]. However, albeit providing micrometer spatial resolution and a very high angular sensitivity, the grating interferometry method is only suitable for measuring rather small wavefront curvatures [8,9]. Large phase differences between a pair of neighboring points in the CRL exit plane will produce ambiguous shift of fringes, which give rise to the phase wrapping problem. Increase of the grating pitch will reduce the sensitivity. For these reasons, the interferometer has been used to study aberrations of a unit X-ray lens only [7,10]. To cope with large wavefront curvatures induced by a stack of unit X-ray lenses we employed a double crystal setup (DCS) method [11,12]. This method consists in detecting the shift of the double crystal rocking curve when a refractive object is placed between two crystals. We exploited the fact that DCS technique can be straightforwardly applied to characterize the beam wavefront at a very high X-ray energy. The generalized pupil function at typical working energies of CRLs can be obtained then by an appropriate scaling of the measured wavefront slopes and transmission. Such scaling is possible as discussed in Section 4. Following this approach, we carried out measurements at  $E = 90$  keV where angular deflections of X-rays are on the order of several microradians even after they have traversed

through tens of unit X-ray lenses. Owing to very small angular deflections, X-rays do not experience large transversal displacements upon propagation from CRL to the detector, which is positioned as close to the CRL as possible. Thus, each detector pixel is unambiguously associated with a point in the CRL exit plane. In this way  $T$  and  $\phi$  can be measured with a fine spatial resolution.

## 2. Sample and experimental details

Tested lenses were produced by the Technological Institute for Superhard and Novel Carbon Materials (TISNCM) in Troitsk, Russia (see [4] for details on the growing process and laser micromachining). The unit lenses are plano-concave. Concave lens surfaces are defined by a paraboloid of revolution with the radius of curvature  $R_l = 200 \mu\text{m}$  at its vertex. The unit lens thickness was approximately 0.5 mm and the diameter of the geometric lens aperture is equal to 0.9 mm. CRL was assembled by pressing  $N = 9$  lenses one after another into a guiding duct drilled in an acrylic puck. Optical microscope was used to confirm that there are no debris such as plastic curls in the CRL pupil [Fig. 1(b)]. The concave surface appears as almost optically opaque, round area due to graphitization of surface layer, which takes place during ablation. Theoretical optimal performance of a diamond CRL is achieved around 15 keV. At this energy ratio of the real part of the refractive index to the attenuation coefficient is close to maximum.

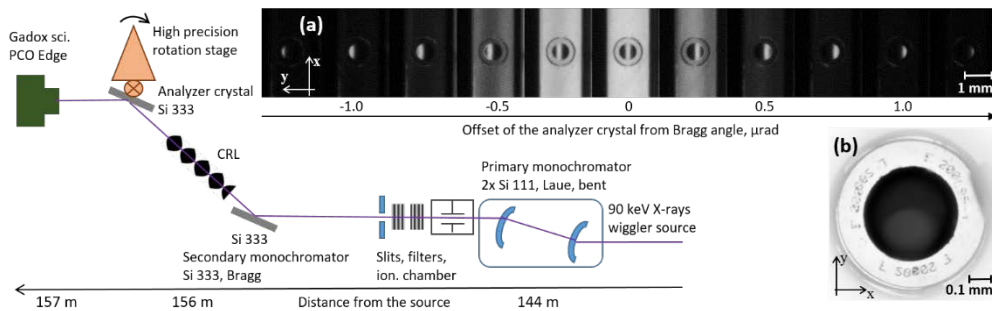


Fig. 1. Experimental setup: in-vacuum Si (111) Laue monochromator reduces relative energy bandwidth to  $\Delta E/E \sim 10^{-3}$ ; the first Si (333) crystal of DCS reduces  $\Delta E/E$  to  $\sim 10^{-5}$ . Divergence of the beam in the CRL entrance pupil is  $\sim 6 \times 10^{-6}$   $\mu\text{rad}$  owing to the large distance to the source. Divergence of the beam in the analyzed  $21 \times 21 \mu\text{m}^2$  wavefront samples is much smaller than the rocking curve width of the Si (333) reflection. Inset (a) shows X-ray images of the CRL versus position of the second, analyzer crystal. An optical image of the CRL pupil is shown in (b).

Measurements were carried out at biomedical beamline ID17 of the European Synchrotron Radiation Facility (ESRF, France). The experimental station is situated 150 m far from the source (Fig. 1). A collimated (divergence  $\sim 6 \mu\text{rad}$ ), monochromatic (relative energy bandwidth  $\approx 10^{-5}$ ) X-ray beam probes a CRL placed between two planar, perfect Si crystals operating in (333) reflection. Comparing to this reflection, the relative intensities of the lower and the most intense, higher order reflections are  $\leq 10^{-4}$  and thus can be neglected. The intensity  $I_{RC}$  of the beam transmitted through the CRL is measured after reflection from the second (analyzer) crystal as a function of the crystal angle  $\theta$  and spatial coordinates:  $I_{RC} = f(\theta, x, y)$ . The angle  $\theta$  is equal to the deviation of the analyzer crystal from the exact Bragg angle for the given beam energy; the  $(x, y)$  coordinates describe both a point in the CRL exit plane and the detector pixel corresponding to that wavefront sample. If  $\theta = 0$  only those rays which have not experienced vertical deflection will contribute to the image. In order to reflect a peripheral ray, which experienced the largest angular deflection, one needs to detune the analyzer crystal from the initial position  $\theta = 0$  in order to meet the Bragg condition [Fig. 1(a)]. The amount of rotation  $d\theta$ , at which intensity in each detector pixel is maximized, is

equal to the vertical component of the angular deflection  $\alpha(x,y)$  of X-rays in a wavefront sample corresponding to that pixel. Total deflection of X-ray can be computed from two orthogonal components. To obtain the horizontal component, the CRL is rotated by a right angle around its optical axis and measurement of the rocking curves is repeated. In this way, the refractive properties of a sample placed between two crystals can be assessed. In addition, the integration of the rocking curve function  $I(x,y)$  over  $\theta$  and comparison with the same quantity obtained without the lens placed in between the crystals yields information about attenuation of the beam [12].

The X-ray detector (PCO.Edge.5.5 camera connected with a 1:3.6X optics to a Ga-based scintillator) provided an effective pixel size of  $21 \times 21 \mu\text{m}^2$  to ensure that the dimensions of the analyzed wavefront samples significantly exceed both the first Fresnel zone and the transversal displacement of X-rays, experienced by them upon propagation from the CRL to detector. The distance between the sample and detector was around 1 m; that determines the diameter of the first Fresnel zone of about  $3 \mu\text{m}$ , so that diffraction effects can be neglected for the selected pixel size. Taking typical deflection angles, one obtains that the largest transversal displacement of the rays should be around  $1 \mu\text{m}$ . Therefore, to a very good approximation, wavefront fragments associated with each pixel can be analyzed independently of each other.

In practice, intensity and angle of incidence of X-rays changes at different points in the CRL entrance plane. In order to account for the spatial variations of parameters of the probing X-ray beam a reference rocking curve was acquired without the sample. The deflection and attenuation of X-rays at different points at the CRL exit plane is evaluated then by comparing rocking curves recorded with and without the CRL placed between two crystals.

### 3. Measurement results

Measured magnitudes of the vertical component of the X-ray deflection and of the CRL transmission  $T$  are shown in Figs. 2(a) and 2(b) correspondingly. Figure 2(c) shows the X-ray deflection in the sagittal and meridional planes of the CRL (note that X-rays experience only horizontal and only vertical deflection in the sagittal and meridional planes respectively). The results clearly show that the CRL does not refract X-rays perfectly: the difference between deflection produced by an ideal parabolic CRL and measured values is shown by red markers in Fig. 2(c). There are deviations from a perfect line, which become more pronounced at the peripheral part of the lens exit pupil. The error profile exhibits rotation symmetry: its shape has similar appearance along any diameter. The slope of the line, which minimizes the error between observed and expected deflection angles, corresponds to a parabolic profile with parameter  $R = 215 \mu\text{m}$ . The effective radius of curvature is thus larger than the designed value  $R_t = 200 \mu\text{m}$ .

The two orthogonal components of the X-ray deflection angle were combined to retrieve the phase delays introduced by the CRL [13]. The reconstructed wavefront is shown in Fig. 2(e). The phase difference  $\phi(x,y)$  between the observed aberrated and the ideal parabolic wavefronts is shown in Fig. 2(f). Upon integration the systematic deviation of deflection angles from ideal values [Fig. 1(c)] is converted to non-monotonic phase error profile, which also exhibits rotation symmetry. It can be seen that at radial distances from CRL optical axis lying in the range  $100 < r < 200 \mu\text{m}$ , the phase delay is smaller than expected. The wavefront advances too much, which means that the projected thickness of diamond is increasing faster than necessary. At  $r \approx 200 \mu\text{m}$  there is an inflection point and outside this circle  $\phi(x,y)$  monotonically and rapidly increases in all radial directions. That means that the projected thickness of diamond is smaller than expected at the peripheral part of CRL. It can be explained by an excessive removal of material during the milling procedure. As a result the wavefront curvature is smaller than in a perfect lens similarly to the negative spherical aberration in a visible light lens [14].

#### 4. Energy scaling of the measured pupil function

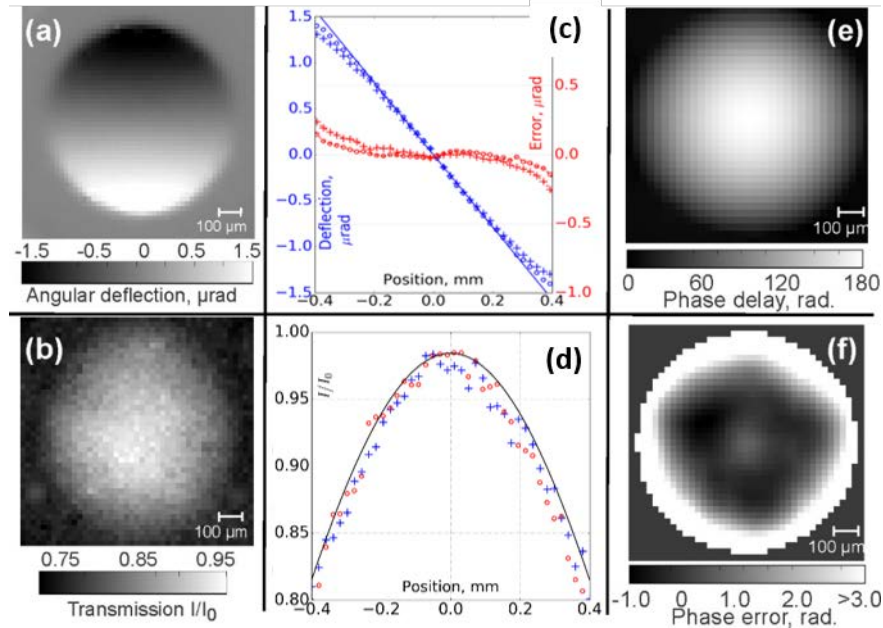


Fig. 2. Experimental results. Two-D maps of the vertical component of the X-rays' deflection angle (a) and transmission  $T$  (b). Panels (c) and (d) show with different markers deflection angle profiles and  $T$  measured at points in sagittal and meridional planes of the CRL; deflection and  $T$  produced by ideal parabolic profile are shown by solid lines. Right y-axis in panel (c) shows the magnitude of the deflection error plotted with red color. Reconstructed phase delays and deviation  $\phi$  of the phase from a perfect parabolic figure are shown in panels (e) and (f).

Functions  $T$  and  $\phi$  constitute the generalized pupil function of the tested CRL at 90 keV. They can be scaled with X-ray energy and, consequently, be used to evaluate the CRL performance at energies close to typical operation conditions at synchrotrons or laboratory sources.

The phase error  $\phi$  scales inversely to the photon energy, since  $\phi(E) \sim k \cdot \delta \sim E^{-1}$ , where  $k \sim E$  is the X-ray wavenumber and  $\delta \sim E^{-2}$  is the unit decrement of the refractive index [11]. Scaling of the intensity transmission  $T$  is somewhat more complicated. Its dependence on the thickness of the traversed material is described by the well-known Beer-Lambert law  $T(E) = I/I_0 = e^{-\mu(E)t}$ . The transmission measured at 90 keV [Fig. 2(b)] can be thus used to extract the projected thickness of the diamond  $t$ . With the known thickness,  $T$  can be estimated at a lower energy if the attenuation coefficient  $\mu$  is also known. For the perfectly homogeneous material  $\mu$  can be derived from the cross-sections of the elementary interactions. However, the effective attenuation coefficient can be larger than the tabulated value if X-rays are additionally scattered on microscopic inhomogeneities, which can exist in the CRL volume. To this end, we have compared the measured transmission against the theoretical one. The theoretical estimate was made using the NIST tables for the diamond density of  $3.54 \text{ g/cm}^3$ . It can be seen from Fig. 2(d) that the measured transmission closely matches the theoretical value. Therefore, we assume that the decrease of transmission due to the small angle X-ray scattering on inhomogeneities inside the CRL can be neglected. Consequently, an estimate of  $T$  at a lower X-ray energy  $E'$  was obtained by extracting the diamond thickness from the measured  $T(90\text{keV})$  and substituting it into the Beer-Lambert formula with  $\mu = \mu(E')$ .

The scaling of the real part of refraction index  $\delta \sim E^{-2}$  is exact for any energy that is far above the K-edge of the CRL material. Therefore the phase delays and refraction angles can be converted to a lower energy without errors. However, observed minute differences

between theoretical and measured transmission may change in a more complicated way than the simple energy scaling law suggests for the small angle scattering. The scaling of the CRL transmission function considered here provides an upper estimate for the transmission at lower energy.

## 5. Applications of the measured pupil function

After having established the scaling procedure for the generalized pupil function, we applied the measured  $P$  to evaluate performance of the CRL at  $E = 15$  keV. First, we have computed its point spread function (PSF). The PSF is an important metric considering that in practice the spatial coherence of the X-ray beam illuminating a CRL is often much smaller than its aperture. The PSF indicates the degree of blurring in the image of a point source. We computed the PSF by applying the inverse Fourier transform to the autocorrelation of the generalized pupil function [6]. Figures 3(a)–3(c) illustrate the effect of optical aberrations on the PSF shape. It is seen that the full-width of the PSF central peak computed taking into account optical aberrations is nearly twice larger than the width of the PSF estimated solely from the CRL transmission (solid and dashed lines in Fig. 3(c) respectively). This indicates that the image of the point object or focal spot of collimated beam will be larger than it might be predicted basing on the transmission.

The measured X-ray deflection angles and the retrieved generalized pupil function can be also used to compute the intensity of a synchrotron radiation beam at various distances after the CRL. In this way, parameters of the focused beam can be evaluated. Measured deflection angles can be used as boundary condition for ray-tracing calculations within the geometrical optics approximation (GO) while retrieved distribution of the phase delays can be used to simulate the beam propagation using the wave optics approach. For the sake of demonstration we assume that the CRL is illuminated by a parallel, monochromatic, 15 keV X-ray beam. To set up the ray-tracing, measured deflection angles and the lens transmission, appropriately rescaled for selected energy, were used as the boundary conditions in the lens exit plane. Propagation of the wavefront was computed with the angular spectrum method [6]. Oversampling of the measured pupil function, required to avoid aliasing errors, was done without smoothing so that the genuine features of the aberrated wavefront were not distorted. An aperture with the opening radius  $r = 250$   $\mu\text{m}$  is set in the entrance pupil to cut off the peripheral part of the lens, where aberrations are particularly strong.

GO predicts that the circle of least confusion is located in the plane  $z = 710 \pm 10$  cm [Fig. 3(d)], whereas the theoretical focal plane position is  $z_t = R_t/(N \cdot \delta) = 680$  cm. Apparently, a smaller focal spot and larger peak intensity can be achieved by shifting the observation plane away from the CRL. This is in a good agreement with the results of Section 3. The focal spot computed using the extracted phase and the angular spectrum method is also found downstream from the expected position at  $z = 700 \pm 10$  cm. Intensity of the beams in the focal plane is shown in Figs. 3(e) and 3(g). In both cases, the focal spot full width taken at half-maximum of the beam intensity is  $\approx 12$   $\mu\text{m}$ . Inside this spot  $\approx 70\%$  of the transmitted beam intensity is contained [Fig. 3(h)]. Good agreement between the GO ray tracing and wave optics is explained by the fact that influence of aberrations on the beam propagation is much stronger than the effect of diffraction on the CRL aperture.

In the synchrotron radiation applications the intensity gain parameter  $G$  is typically considered. It can be defined as the ratio of the beam intensity in the focal spot of the lens to the intensity at the same area without the CRL. Our numerical study shows that  $G \approx 1100$  in the corrected focal plane, whereas the gain computed at the distance  $z_t$  is only equal to 700. The maximum achievable gain for  $r = 250$   $\mu\text{m}$  aperture is 1500, given that the average CRL transmissivity at this energy is  $\approx 0.85$ . It can be concluded that due to the wavefront aberrations the achievable gain is reduced by about 30% if the inner part of the CRL is used. The gain does not change substantially for a wider opening of the aperture because of the strong peripheral aberrations. Figures 3(e) and 3(f) compare beam intensities calculated for

CRL apertures  $r = 250 \mu\text{m}$  and  $400 \mu\text{m}$  respectively. In the latter case the beam is larger, but the intensity values near the peak are nearly identical to the former case.

It must be noted that in this experiment we were not able to resolve any features with spatial scales smaller than the detector resolution. In practice, such inhomogeneities will affect the distribution of intensity in the focal spot. This information, however, is not completely lost. Scattering and multiple refraction of X-ray on sub-pixel inhomogeneities increase the width of the rocking curve and decrease its peak and integrated intensities. The noisiness of the attenuation profile in Fig. 2(b) exhibit random deviations of the CRL transmission from the theoretical profile. One can think of it as the increase of the attenuation coefficient due to additional scattering on unresolved microscopic inhomogeneities inside the CRL and residual surface roughness. Increase of the rocking curve width could provide an estimate for the dispersions of the deflection angles caused by subpixel inhomogeneities.

It is also necessary to note that recently aberrations in a CRL have been successfully measured using ptychography technique [15]. Although ptychography provides an unprecedented spatial resolution, presented here DCS method has an important advantage: characterization can be performed directly in the CRL exit plane. Thus, regardless of how large the CRL focal length is, the quality of a CRL can be assessed prior to its installation at the final position in the beamline. Moreover, measurements with DCS setup can be performed even with a laboratory source, if the probing beam divergence is appropriately reduced by means of an asymmetrically cut crystal.

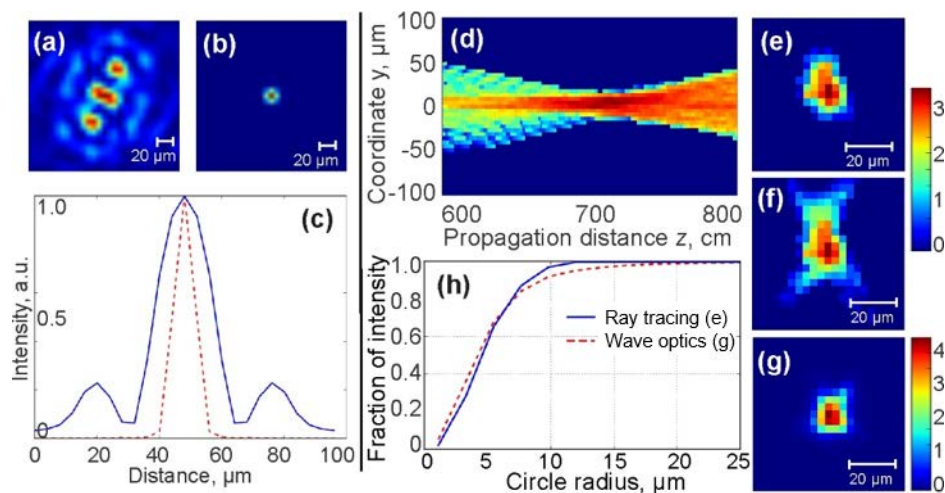


Fig. 3. Applications of the generalized pupil function: panels (a) and (b) show the PSF of the CRL calculated with and without optical aberrations taken into account; 1D profiles of the PSF are compared in (c). Panels (d-g) demonstrate the simulated propagation of the 15 keV photon beam after the CRL. Evolution of the beam intensity along the propagation axis  $z$  (d); intensity in the plane  $z = 710 \text{ cm}$  calculated using GO (e) and wave optics (g). To illustrate that peripheral aberrations limit the gain, intensity of the beam in the focal plane is shown in (f) for the case of fully open CRL aperture. All results are displayed on a uniform grid with  $4 \mu\text{m}$  spacing. Panels (d-f) share the colorbar shown on their right. The intensity of the transmitted beam integrated in the focal plane is equal to 400 a. u. for panels (e,g) and 880 for the case (f). The fraction of the encircled beam intensity in the focal plane against the spot radius is shown in (h). Log scale is shown in all 2D maps.

## 6. Conclusions

We have measured the generalized pupil function of a single crystal diamond refractive X-ray CRL and discussed how it scales with the X-ray energy. This function can be used to assess the quality of a CRL. For instance, calculated PSF of the examined CRL indicates that wavefront aberrations significantly deteriorate the attainable focal spot size and the

resolution. We have also used the results in numerical simulations in order to estimate the gain that CRL can achieve in a simple case of a parallel beam illumination. Thereby, dimensions of the focal spot, intensity gain, and a number of other important parameters were estimated. Information about the intensity distribution and the wavefront of an X-ray beam generated by a real source can be also included in such simulations.

The double crystal experimental technique used in this work can be used to characterize strong curvatures in X-ray beams with a reasonably high spatial resolution. At 90 keV, the setup of the ESRF ID17 beamline can measure X-ray angular deflections up to  $\pm 30 \mu\text{rad}$ , which is equivalent to  $\pm 1 \text{ mrad}$  for a metrology setup operating at 15 keV. That might prove useful if a direct characterization of refractive properties of an X-ray lens composed of many tens of unit lenses is required.

### **Acknowledgments**

We would like to acknowledge the ESRF for provision of the beamtime through proposals MD912 and IH1227.